

Article

Theoretical Analysis of SAW Propagation in 3C-SiC/c-AlN

Cinzia Caliendo

Istituto di Acustica e Sensori Corbino, IDASC-CNR, Via del Fosso del Cavaliere 100, Roma 00133, Italy; cinzia.caliendo@idasc.cnr.it; Tel.: +39-06-4993-4741; Fax: +39-06-4993-4061

Academic Editor: Helmut Cölfen

Received: 31 December 2015; Accepted: 10 March 2016; Published: 15 March 2016

Abstract: The anisotropic materials as the acoustic wave propagating medium introduce the dependence of the phase velocity on the wave propagation direction, as opposed to the isotropic counterparts; in addition, the profile of the particle displacement components can be quite different, depending on the crystal type and propagation direction. The propagation of surface and bulk acoustic waves (SAWs and BAWs) along the (001), (111) and (110) planes of cubic SiC crystals have been studied. For specific propagation directions in these planes, slight variations in the velocity of the elastic surface waves are found. It was observed that Rayleigh-type, generalized and pseudo-surface waves can propagate at specific directions, thus confirming how the anisotropic behavior of the bare SiC substrate modifies the existence and the field profile of the SAW that propagates at its free surface. Finally, the SAW propagation along AlN/SiC-based multilayered structures is studied for the three SiC planes, different AlN piezoelectric layer thicknesses and electrical boundary conditions.

Keywords: 3C-SiC; AlN; anisotropy; SAW; BAW

1. Introduction

Bulk acoustic waves (BAWs) propagating along an anisotropic medium show characteristics different as compared to the isotropic case. For higher symmetry crystals, if the wave propagation direction coincides with the principal axis direction, then three pure modes propagate having their polarization vectors parallel to the reference system axis: the longitudinal, shear horizontal and shear vertical bulk acoustic waves (LBAW, SHBAW and SVBAW). Nevertheless, for an arbitrary propagation direction, the polarization vector of the three bulk waves is neither necessarily parallel nor normal to the slowness vector: the *quasi* longitudinal and the two *quasi* shear waves show three displacement vector components. Surface acoustic waves (SAWs) propagating in isotropic media are elliptically polarized in the sagittal plane (the plane perpendicular to the free surface and containing the propagation vector): their phase velocity is unaffected by the propagation direction, and, consequently, the phase and group velocities coincide. On the contrary, the properties of the SAWs propagating along an anisotropic medium are mainly constrained by the crystallographic orientation of the free surface and by the direction of propagation. The SAWs show, in general, three displacement components, and the phase velocity depends on the propagation direction and does not coincide with the group velocity. Moreover, for specific propagation directions, the SAW, in its more general definition, does not exist and unconventional surface waves propagate, such as leaky or pseudo SAWs (PSAWs). Therefore, the anisotropic behavior of the medium affects the BAW characteristics, and considerably modifies the existence and the structure of the SAW that propagates at its free surface.

In the present paper, the propagation of BAWs and SAWs along the (001), (111) and (110) surfaces of bare SiC cubic crystals (3C-SiC) is studied. Specific directions were found suitable for the propagation of slow and fast *Rayleigh-like* waves, generalized SAWs, and pseudo-SAWs. Moreover, the SAW propagation along 3C-SiC/c-AlN-based multilayered structures is studied for propagation directions

suitable for SAW device applications; different piezoelectric layer thicknesses and electrical boundary conditions were examined. This specific combination of materials was chosen for its suitability for applications in wireless communications and harsh environment sensing fields [1–5], such as extremes of pressure, temperature, shock, radiation and chemical attack. The piezoelectric AlN overlay material has excellent piezoelectric properties, low conductivity, and behaves elastically isotropic for surface waves propagating over the basal plane, provided that the AlN *c*-axis is perpendicular to the SiC substrate surface. The application of the largely-explored piezoelectric AlN film technology, together with the early-developed 3C-SiC film technology [6,7], have just produced some remarkable results [8–10], but, since the SiC technology is far from being mature, many more benefits will be attempted. Bulk SiC production is still in progress while SiC *film* on Si substrates are commercially available even if for limited thickness range. In 3C-SiC/*c*-AlN-based electroacoustic devices, the SiC anisotropy strongly affects the characteristics of the acoustic waves propagation rather than the *c*-AlN that is isotropic in the *c* plane. Hence the propagation characteristics are influenced by the SiC thickness, cut and propagation direction. AlN, which shows the highest SAW velocity between the piezoelectric materials that can be grown in thin film form, has been successfully used in SAW devices operating to gigahertz frequencies. Thus, AlN, in combination with a fast substrate material such as SiC, creates new and exciting opportunities for miniaturizing, reducing power consumption, and improving the performance and functionality of many devices including sensors, actuators, radio frequency micro-electro-mechanical systems (RF MEMS) and optical arrays. Such 3C-SiC/*c*-AlN devices are robust, providing improved chemical stability, thermal stability, reproducibility and sensitivity compared to conventional polycrystalline piezoelectric MEMS.

2. BAW and SAW Propagation in 3C-SiC

A mathematical model was built based on the partial differential equations system derived from the fundamental equations of motion in an elastic, lossless, homogeneous, anisotropic medium [11]. By solving the system of equations, the velocity of the bulk waves propagating along an arbitrary direction was obtained. Because of the anisotropy of the 3C-SiC, the eigenvalues and eigenvectors of the Christoffel's equation were affected by the arbitrary choice of the wave propagation direction. Thus, the phase velocities and the amplitudes of three acoustic modes were obtained for each propagation direction: one wave with longitudinal (or *quasi*-longitudinal) polarization and two waves with transverse (or *quasi*-shear vertical and *quasi*-shear horizontal) polarization [12]. A computer program was developed with Matlab software to determine the acoustic properties of the BAWs propagating along an arbitrary direction of an unbounded, homogeneous, lossless, linearly elastic anisotropic medium. The material constants of 3C-SiC substrates were those indicated in [13]. The theoretical analysis of SAWs characteristics in 3C-SiC was accomplished by solving the continuum equations of motion, the strain-mechanical displacement relations, and the appropriate boundary conditions (traction free boundary conditions at the surface of the half space).

2.1. The (001) Plane of 3C-SiC

The phase velocity of the surface and bulk acoustic waves propagating in the (001) plane of 3C-SiC was calculated for different propagation directions, as shown in Figure 1.

The SAWs and BAWs have the propagation vector lying in the (001) plane of SiC, in the direction indicated by the abscissa of the graph shown in Figure 1. At 0° from the <100> direction, as well as at 90°, the velocity of the two shear bulk waves coincides. The SVBAW is a pure mode polarized along the normal to the (001) plane for every propagation direction in the plane; the SHBAW and LBAW, except at 0°, 45° and 90°, are *quasi*-longitudinal and *quasi*-shear horizontal. With increasing the angle from the <100> direction, the SHBAW velocity decreases and becomes comparable to the velocity of the SAW, while the SVBAW velocity remains constant. For angles off *x*-axis greater than 45°, the SHBAW velocity increases and again coincides with the SVBAW velocity at 90°. The velocity of the LBAW increases for angles from 0° to 45°, and decreases for angles greater than 45° up to 90°.

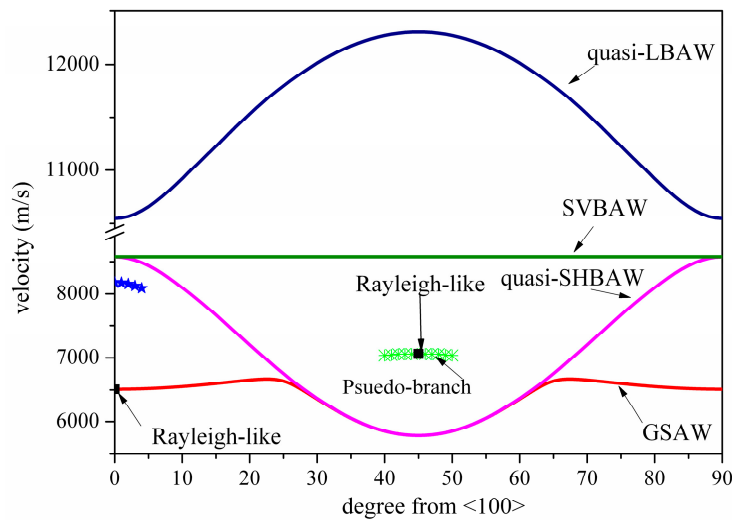


Figure 1. The angular dispersion of the BAWs and SAWs propagating in the (001) plane of 3C-SiC.

At 0° and for few angles neighboring with this direction, the shear bulk wave satisfies the traction free boundary conditions: the wave travels at velocity $v = 8181$ m/s (the blue stars in Figure 1), and the particle displacement is in the sagittal plane, but it is not a surface wave since the wave amplitude does not decay with depth [12], as shown in Figure 2.

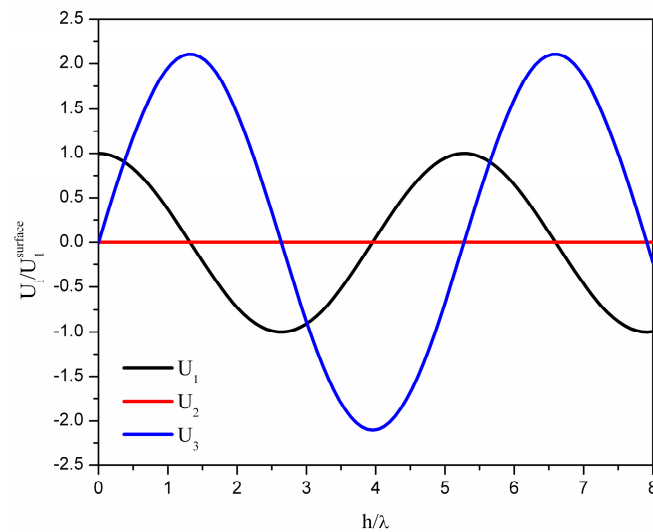


Figure 2. The normalized particle displacement components of the BAW that satisfies the traction free boundary conditions for the $\langle 100 \rangle$ direction in 3C-SiC(001) at velocity $v = 8181$ m/s.

At 0° from the $\langle 100 \rangle$ direction, the SAW travelling at $v = 6510$ m/s is a *Rayleigh-like* wave: the two particle displacement components, the longitudinal and vertical components U_1 and U_3 , show a damped oscillatory nature with depth [12], as shown in Figure 3. The *Rayleigh-like* mode polarization is elliptical with the ellipse lying in the sagittal plane and having the principal axis perpendicular to the free surface: U_1 and U_3 , are in phase quadrature with each other, and the power flux is collinear with the propagation vector.

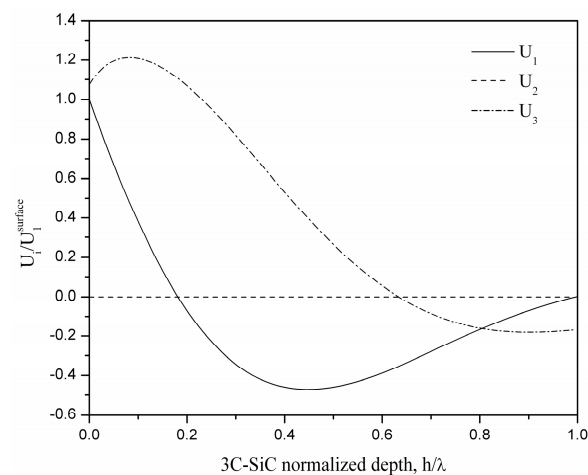


Figure 3. The particle displacement components of the *Rayleigh-like* wave propagating along the x -axis in 3C-SiC(001).

As the propagation vector is rotated from the $\langle 100 \rangle$ direction, the *Rayleigh-like* wave evolves to a generalized surface wave (GSAW) with three particle displacement components U_1 , U_2 and U_3 . When the propagation vector approaches approximately 33° off the $\langle 100 \rangle$ direction, the GSAW velocity becomes comparable to that of the *quasi*-SHBAW and the U_2 component increases rapidly: from here on, the GSAW becomes leaky and degenerates in a bulk shear wave. At 45° off the $\langle 100 \rangle$ direction, there are two eigensolutions to the traction free boundary condition at the (001) plane of 3C-SiC. One solution is a *Rayleigh-like* wave travelling at velocity $v = 7060$ m/s higher than that of the slowest shear bulk wave (5785 m/s); this upper solution has the same characteristics of the *Rayleigh-like* wave solution at 0° and they both show a zero power flow angle (PFA) since the group and the phase velocity are collinear [12]. The lower solution at $v = 5785$ m/s is a wave with a dominant U_2 displacement component almost independent on the depth. Figure 4 shows the displacement components depth profile of the upper solution.

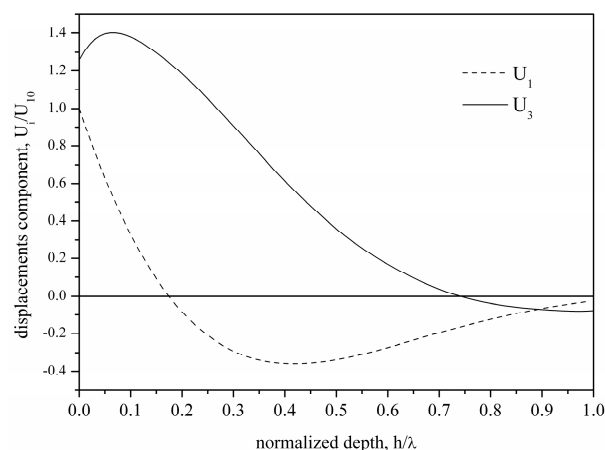


Figure 4. Variation of the normalized vertical and longitudinal displacement components with depth for the *Rayleigh-like* wave propagating along the $\langle 110 \rangle$ direction of the (001) plane of 3C-SiC at velocity $v = 7060$ m/s.

For angles neighboring with the upper solution, except at 45° , a generalized surface wave propagates having three displacement components that become appreciable at greater and greater depths, and hence the wave radiates energy into the bulk. These waves are called “pseudo SAW” (PSAW) [12]. As an example, Figure 5a shows the normalized particle displacement components of the

PSAW propagating at 49° off the $\langle 100 \rangle$ axis: while the U_1 and U_3 components decay with the depth, the U_2 component does not decay and is responsible for the acoustic energy radiated into the bulk of the substrate. Figure 5b shows the PSAWs velocity and propagation loss per wavelength along the propagation direction *vs.* the angle off the $\langle 100 \rangle$ direction: as it can be seen, the propagation loss is zero at 45° off $\langle 100 \rangle$ where a SAW propagates, while it increases when the wave vector is rotated from the $\langle 110 \rangle$ direction.

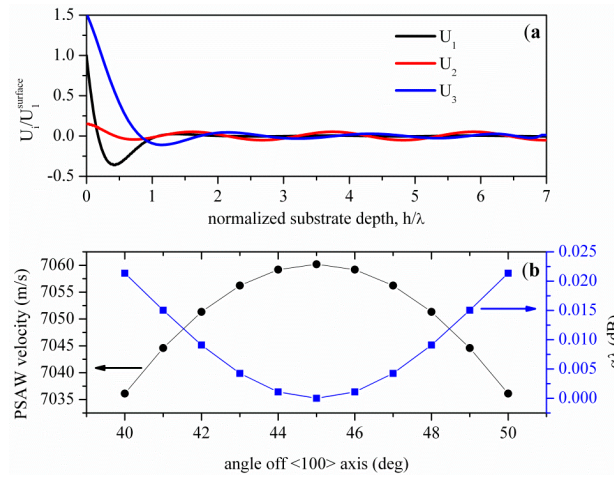


Figure 5. (a) Variation of the normalized shear and longitudinal displacement components with depth for the PSAW propagating at 49° off the $\langle 100 \rangle$ directions of the (001) plane of SiC; (b) the PSAWs velocity and propagation loss *vs.* the angle off the $\langle 100 \rangle$ direction of the (001) plane of SiC.

2.2. The (111) Plane of 3C-SiC

The SAWs and BAWs angular velocity dispersion curves in the (111) plane of 3C-SiC are shown in Figure 6; the curves have mirror symmetry about the 30° direction and hexagonal symmetry on this surface. At 0° from $\langle 110 \rangle$ direction, the three BAWs have equal phase and group velocity, as well as at 60° , with zero PFA. The LBAW is pure while the two shear waves are *quasi*-SHBAW and *quasi*-SVBAW. With increasing the angle, the three BAWs become *quasi*-longitudinal and *quasi*-shear: their displacement components are mixed and their PFA is not zero. At 60° off, the $\langle 110 \rangle$ direction the LBAW is pure as for 0° ; the SHBAW is pure at 30° and 90° , but its phase velocity differs from the group velocity, unlike at 0° . The SVBAW is not a pure mode for any angle, but its phase velocity equals the group velocity at 0° and 60° .

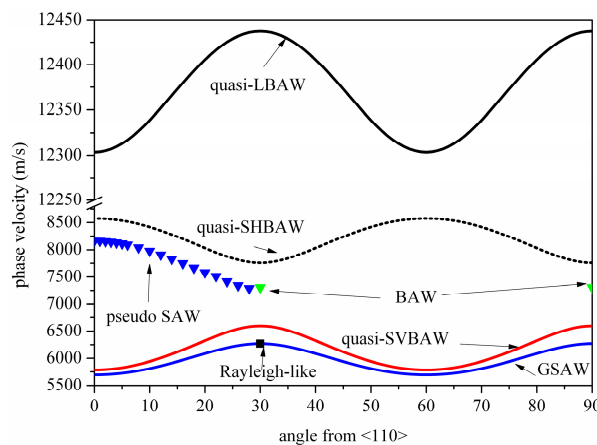


Figure 6. The angular dispersion curves of the SAWs and BAWs propagating along the (111) plane of 3C-SiC.

For SAW propagating along 0° (the $\langle 110 \rangle$ direction, that is normal to a plane of mirror symmetry) the surface displacement ellipse has its minor axis parallel to the direction of propagation while the other principal axis is not perpendicular to the free surface. The plane of the ellipse is rotated some 26° out of the sagittal plane on the free surface. The SAW velocity (5695 m/s) is only about 1.6% below the lowest BAW velocity (5785 m/s) in the same direction and has three displacement components. The penetration of this solution into the bulk of the material is larger than most solutions that are leaky at $h/\lambda = 1$: at one wavelength depth, the present solution shows $U_1/U_{1\text{surface}} = 0.037$, $U_2/U_{1\text{surface}} = 0.79$ and $U_3/U_{1\text{surface}} = 1.1$, as shown in Figure 7a.

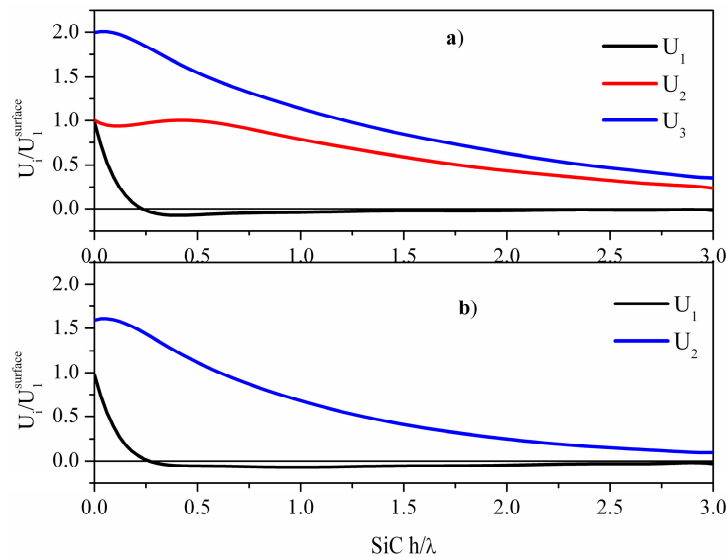


Figure 7. Variation of the normalized shear and longitudinal displacement components with depth for the SAW propagating along the $\langle 110 \rangle$ direction (a) and 30° off the $\langle 110 \rangle$ direction (b) of the (111) plane of 3C-SiC.

Between 0° and 30° , the surface acoustic wave is a GSAW with three displacement components. At 30° in the (111) plane, the surface displacement ellipse lies in the sagittal plane as for a *Rayleigh-like* wave ($U_2 = 0$ and U_1 and U_3 have oscillatory damped behavior, as shown in Figure 7b), but the ellipse major axis is not vertical (the angle between U_1 and U_3 is not 90° but 105° from the U_1 direction, *i.e.*, the propagation direction).

Between 0° and 30° , PSAW propagates at higher velocity than that of the SAW, having three displacement components that are not confined to the vicinity of the surface: the penetration depth of this waves increases gradually with increasing the propagation angle off the $\langle 110 \rangle$, and the PSAW radiates energy into the bulk. Figure 8a–d show the field profile of the PSAW travelling at 0° , 10° , 20° and 25° off the $\langle 110 \rangle$ direction, at velocity equal to 8161.75, 7972.96, 7523.64 and 7370.43, and with propagation loss equal to 0.017, 0.26, 0.54 and 1.08 dB per wavelength, respectively. As it can be seen, with increasing the angle from the $\langle 110 \rangle$ direction, the penetration into the bulk gradually increases. At 30° (as well as at 90°), the pseudo SAW degenerates in a SHBAW having only one displacement component (U_2).

2.3. The (110) Plane of 3C-SiC

Figure 9 shows the phase velocity angular dispersion curves of the BAWs and SAWs propagating in the (110) plane of 3C-SiC. At 0° from the $\langle 001 \rangle$ direction in the (110) plane, as well as at 180° , the two bulk shear waves travel at the same velocity (8577 m/s): at this specific direction, the phase and group velocities of the three BAWs coincide. With increasing the angle off the $\langle 001 \rangle$ direction, the longitudinal wave becomes *quasi*-longitudinal and becomes again a pure mode at approx. 51° up to

90° off <100>. The *quasi*-SHBAW, having approximately mirror symmetry about 45°, has its particle displacement components in the (110) plane at all angles, and is a pure mode in the range from ~51° to 58° and at 90°, whereas the SVBAW has its displacement component perpendicular to this plane at all angles.

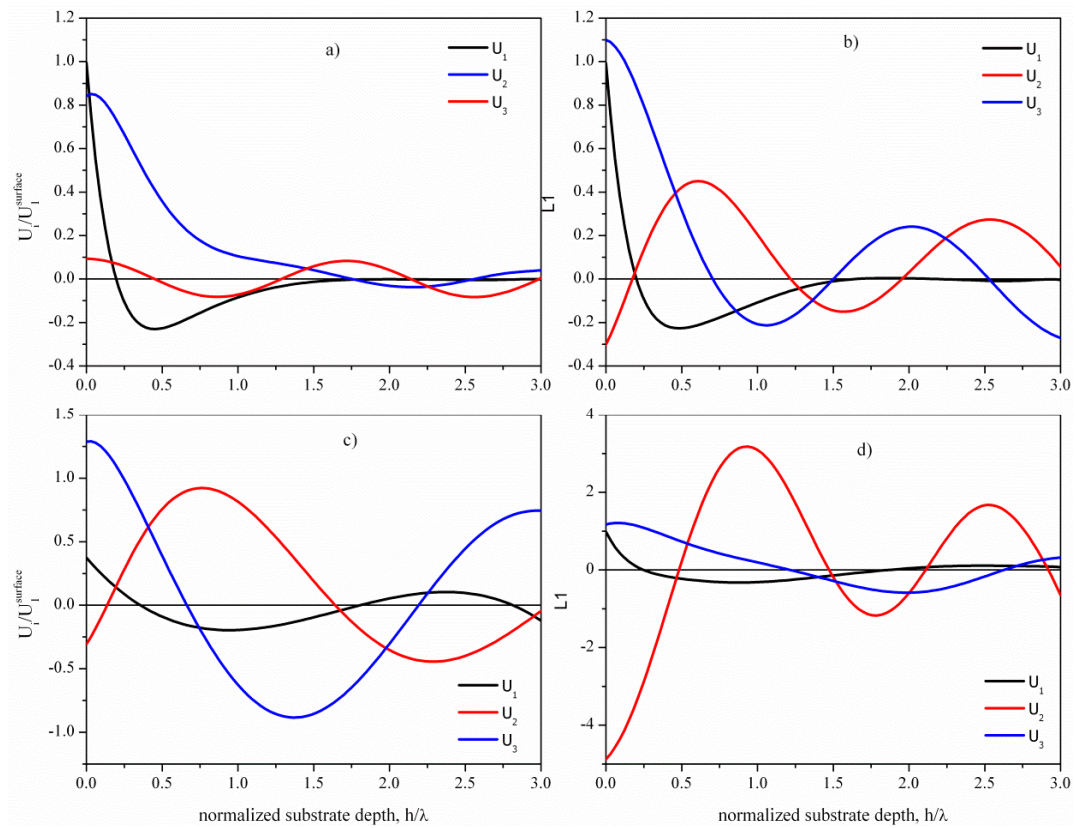


Figure 8. The field profile of the pseudo SAW travelling at: 0° (a); 10° (b); 20° (c) and 25° (d) off the <110> direction of the (111) plane of 3C-SiC.

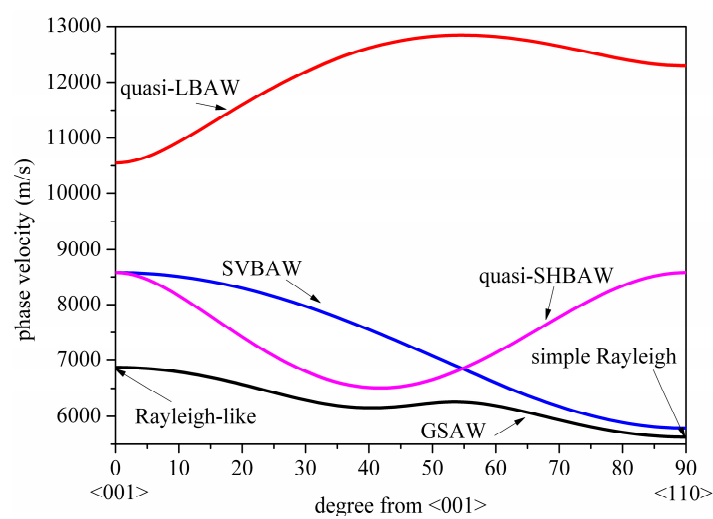


Figure 9. The phase velocity angular dispersion curves of the BAWs and SAWs propagating in the (110) plane of 3C-SiC.

Along the $\langle 001 \rangle$ direction of the (110) plane, a Rayleigh-like mode propagates with two displacement components U_1 and U_3 vanishing with depth in an oscillatory way, as shown in Figure 10a. Along the $\langle 110 \rangle$ direction, a *simple Rayleigh* wave propagates [12] with two displacement components U_1 and U_3 , slowly damping into the bulk, as shown in Figure 10b.

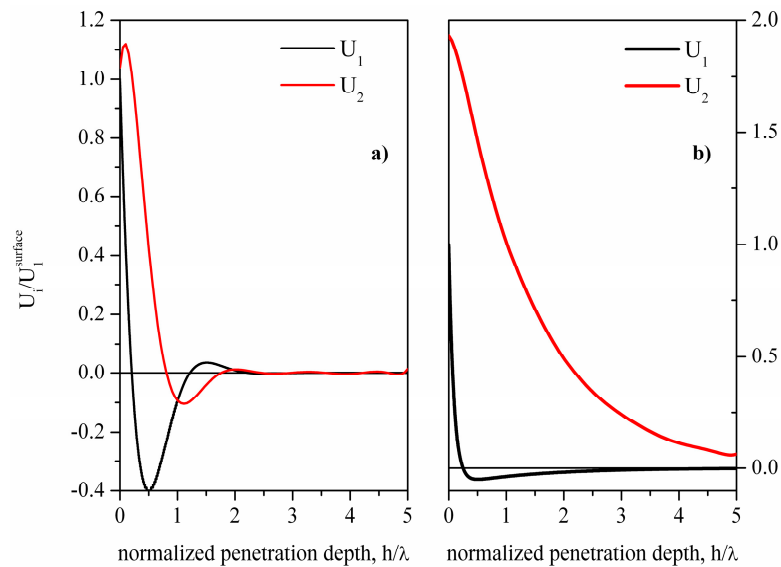


Figure 10. Variation of the normalized shear and longitudinal displacement components with depth of the *Rayleigh-like* wave propagating along $\langle 001 \rangle$ (110)SiC (a) and of the *simple Rayleigh* wave propagating along $\langle 110 \rangle$ (110)SiC (b).

For propagation directions between $\langle 001 \rangle$ and $\langle 110 \rangle$, a GSAW propagates with three displacement components U_1 , U_2 and U_3 . The U_2 component amplitude increases from 0° to 45° off $\langle 001 \rangle$ because of the approaching of the GSAW and SHBAW velocities, while it decreases from 45° to 90° with the increasing of the velocity difference between the GSAW and SHBAW. The U_2 component *vs.* the SiC normalized depth is shown in Figure 11, for different propagation directions in the (110) plane.

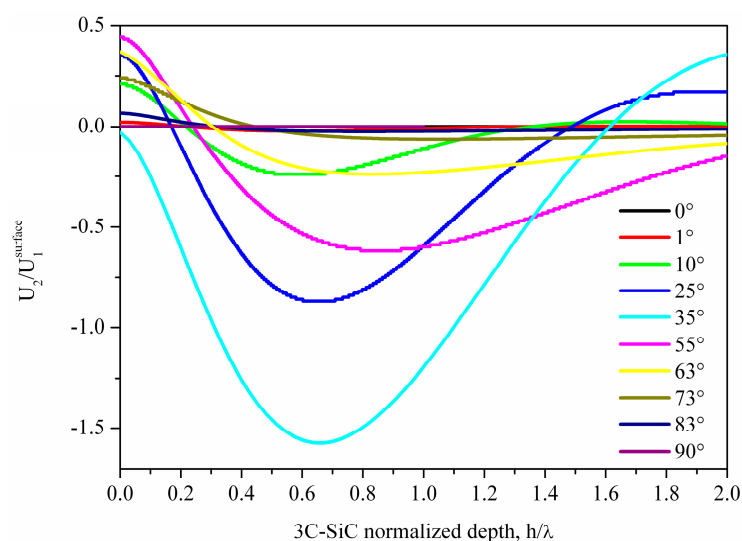


Figure 11. Variation of the normalized shear horizontal displacement component *vs.* the SiC depth, being the angle off the $\langle 001 \rangle$ axis the running parameter.

No degeneration of SAW into a BAW at any angle was observed, and no pseudo surface-branch appeared. It is worth noting that the SHBAW satisfies the traction free boundary conditions for both the $\langle 001 \rangle$ and $\langle 110 \rangle$ directions, even though these solutions do not represent a surface wave.

3. Acoustic Wave Propagation in 3C-SiC/c-AlN

In a film/substrate structure, the acoustic wave propagation properties become dispersive with respect to the thickness of the layer. As a result, in the SiC/AlN multilayer structure, the SAW propagation properties would be dispersive with respect to the AlN film thickness normalized to the wavelength. Moreover, the phase velocity dispersion curves of SAW propagating along different directions in different planes of the SiC substrate covered by an AlN layer are not identical due to the cubic crystal system of the SiC half-space.

The phase velocity dispersion curves of SAW propagating along the (001), (111) and (110) planes of 3C-SiC substrate covered by a piezoelectric c-AlN layer was investigated for different propagation directions and electrical boundary conditions. The electromechanical coupling constant $K^2 = 2 \cdot [(v^f - v^m)/v^f]$, the percentage difference of the velocity between a free surface (v^f) and surface coated with an infinitesimally thin perfect conductor (v^m), is used as direct estimate of surface-wave coupling to interdigital transducers [14,15]. The SAW devices with four types of transducer configurations on the SiC/AlN multilayer structure are studied: the typologies called SFT (substrate/film/transducer) and SMFT (substrate/metal/film/transducer) represent a pair of transmitting and receiving interdigital transducers (IDTs) on the top AlN surface combined with and without a metallized interface in the SiC/AlN structure; the typologies called STF (substrate/transducers/film) and STFM (substrate/transducer/film/metal) represent a pair of IDTs in the SiC/AlN interface joined with a unmetallized and a metallized top AlN surface. In the theoretical calculation, the AlN thin film is treated as a hexagonal crystal system, and the SiC substrate is treated as a cubic crystal system whose thickness is assumed to be infinite. The velocity calculations were performed under the hypothesis of lossless materials, assuming the single crystal AlN and 3C-SiC material constants available in the literature [16,17].

3.1. Surface Acoustic Waves in 3C-SiC(001)/c-AlN

When the 3C-SiC half-space is covered by a thin c-axis oriented AlN layer, the surface wave velocity along the (001) plane of the SiC/AlN becomes dispersive. Both the SiC(001) $\langle 100 \rangle$ /c-AlN and SiC(001) $\langle 110 \rangle$ /c-AlN substrate are a combination of *slow* film on a *fast* substrate as the SAW velocity of AlN is lower than that of the substrate. Since the SVBAW in the film is slower than the SVBAW in the substrate, there exist higher Rayleigh-type modes having a low frequency cut off at which the phase velocity is equal to the substrate SVBAW velocity; with increasing the layer thickness, the velocity of these higher order modes asymptotically reaches the SVBAW velocity in the layer. Figure 12 shows the dispersion curves of the *first* Rayleigh-like mode (with two displacement components, U_1 and U_3) propagating along the $\langle 100 \rangle$ and $\langle 110 \rangle$ propagation directions. For vanishingly AlN thin layer thickness ($h/\lambda \ll 1$), the Rayleigh-like mode velocity equals the *Rayleigh-like* mode velocity in the bare SiC substrate. When the layer thickness becomes large compared to the wavelength ($h/\lambda > 1$), the wave velocity decreases and asymptotically reaches the SAW velocity appropriate to a free surface of the layer material (5607 m/s).

Figure 13a,b show the K^2 dispersion curves of the four coupling configurations for the SAW propagating along the $\langle 100 \rangle$ and $\langle 110 \rangle$ directions of 3C-SiC(001)/AlN.

As it can be seen from Figure 13, the K^2 dispersion curves are strongly affected by the electrical boundary conditions that influence the potential depth profile. For acoustic waves propagating along layered structures, the achievable K^2 can be larger than that of AlN (0.3%) considered as a semi-infinite substrate, due to an increased acoustic energy confinement. Between the four coupling structures, the STFM and STF structures exhibit the highest K^2 value for an AlN normalized thickness equal to about 0.5.

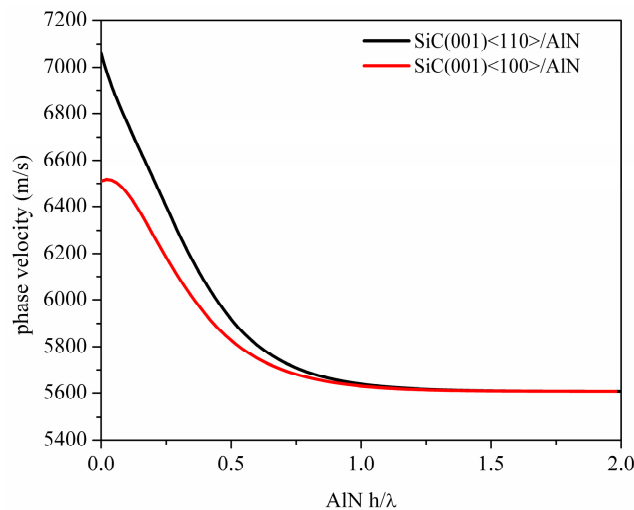


Figure 12. The phase velocity dispersion curves of the *Rayleigh-like* waves propagating along 3C-SiC(001)<100>/c-AlN and 3C-SiC(001)<110>/c-AlN structures.

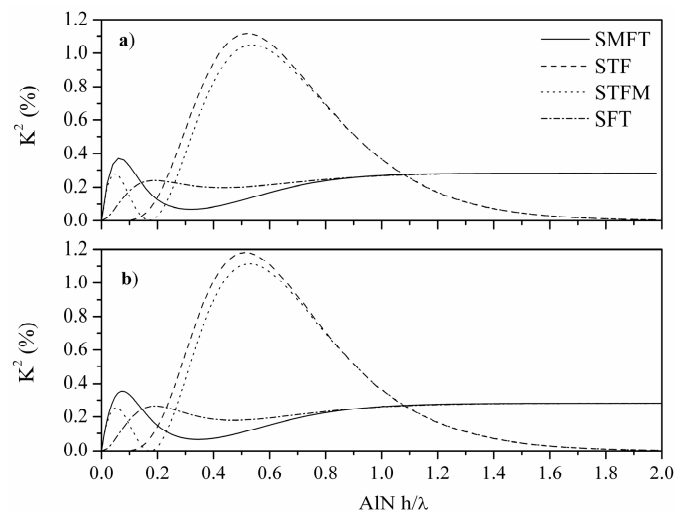


Figure 13. The K^2 dispersion curves of the *Rayleigh-like* waves propagating along the <100> (a) and <110> (b) directions of the four 3C-SiC(001)/AlN-based coupling configurations.

3.2. Surface Acoustic Waves in 3C-SiC(111)/c-AlN

For propagation of SAW at 0° and 30° off the <110> axis, the 3C-SiC/AlN configuration is a *slow on fast* configuration as the SAW velocity in SiC is higher than that in c-AlN. Figure 14 shows the velocity and K^2 dispersion curves of SiC(111)/AlN for propagation along the <110> axis. No higher order modes propagate since the *quasi*-SVBAW velocity in SiC (5784 m/s) is much lower than that of the SVBAW in the AlN (6089 m/s).

Figure 15 shows the velocity and K^2 dispersion curves of SiC(111)/AlN for propagation along 30° off <110> axis. The structure sustains the propagation of higher order modes since the *quasi*-SVBAW velocity in SiC (6597 m/s) is much lower than that of the SVBAW in the AlN (6089 m/s).

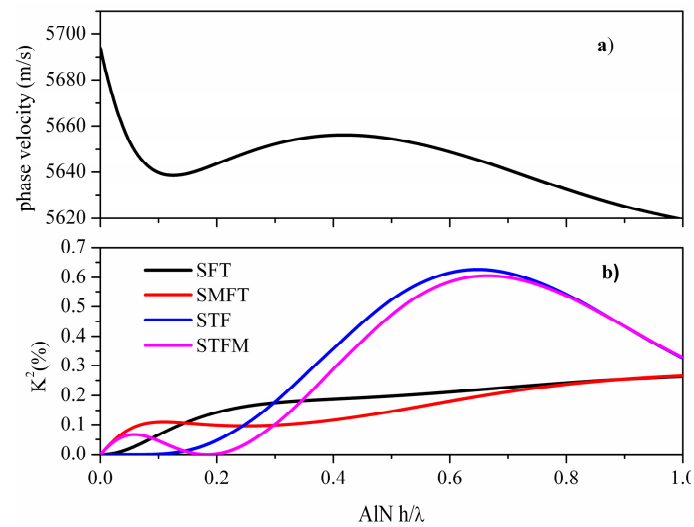


Figure 14. The phase velocity (a) and K^2 (b) dispersion curves for SAW propagating along the <110> direction of the (111) SiC/AlN substrate.

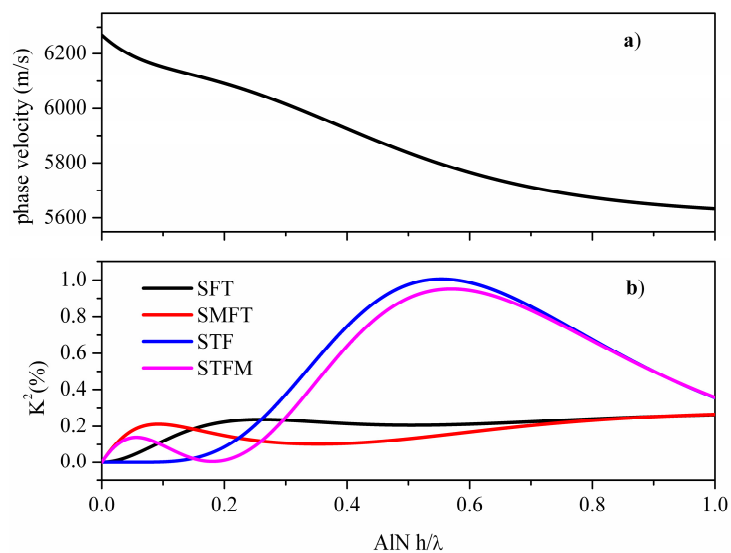


Figure 15. The phase velocity (a) and K^2 (b) dispersion curves for SAW propagating along 30° off the <110> direction of the (111) SiC/AlN substrate.

3.3. Surface Acoustic Waves in 3C-SiC(110)/c-AlN

The phase velocity and K^2 dispersion curves for the fundamental SAW propagating along the <001>(110)SiC/AlN vs. the AlN normalized thickness h/λ are shown in Figure 16a,b.

Such configuration sustains the propagation of higher order modes since the SVBAW velocity of the substrate is higher than that of the AlN layer. The phase velocity and K^2 dispersion curves for the SAW propagating along <110>(110) SiC/AlN vs. the normalized AlN thickness h/λ are shown in Figure 17a,b.

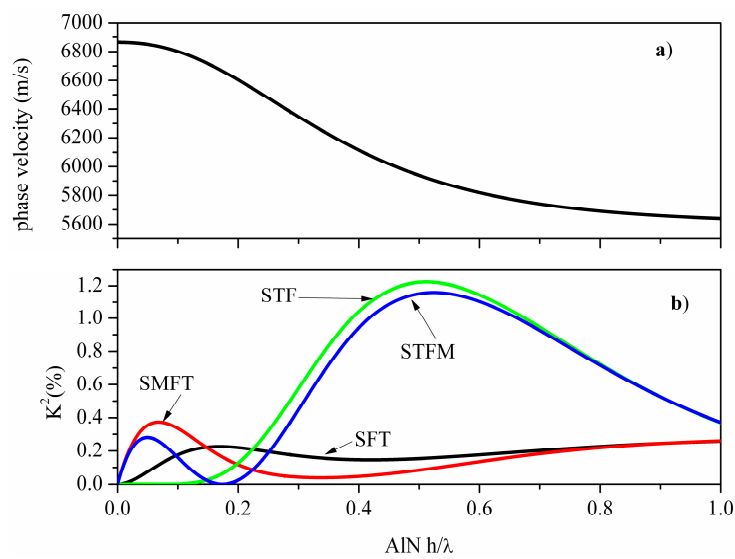


Figure 16. The phase velocity (a) and K^2 (b) dispersion curves for SAW propagating along the $\langle 001 \rangle$ direction of the (110) SiC/AiN substrate.

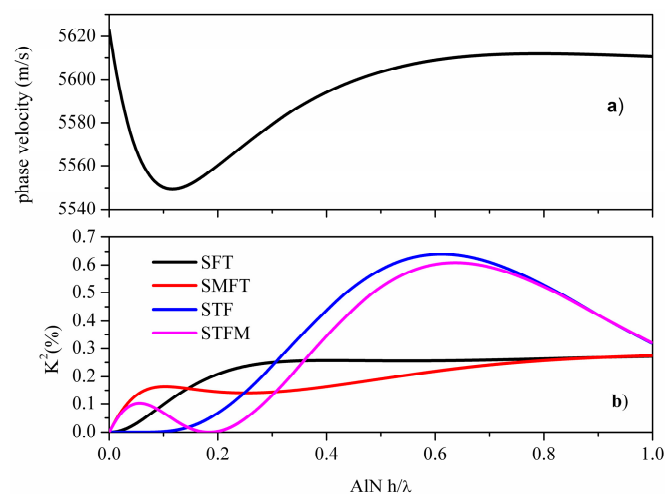


Figure 17. The phase velocity (a) and K^2 (b) dispersion curves for SAW propagating along the $\langle 110 \rangle$ direction of the (110) SiC/AiN substrate.

In this case, no higher order modes exist since the SVBAW velocity in AiN is much higher than that in SiC.

4. Conclusions

The SAW propagation properties through the 3C-SiC/AiN composite structure were theoretically analyzed for different SiC planes, AiN layer thicknesses, acoustic wave propagation directions and electrical boundary conditions. The calculations performed demonstrate the potential of AiN thin films grown on epitaxial 3C-SiC layers to create layered SAW devices with high phase velocity and large electromechanical coupling coefficient. The simulation results show that SAW propagating along the $\langle 110 \rangle$ direction of the (001) plane has the highest phase velocity among the other directions studied: for AiN thickness of about $0.1 \cdot \lambda$, the velocity is about 7000 m/s, with a $K^2 \sim 0.4\%$ for the SMFT configuration; while for an AiN thickness of about $0.5 \cdot \lambda$, the K^2 is about 1.2% and the velocity is about 6000 m/s for the STF configuration. The results conclude that the 3C-SiC/AiN multilayer structure

possesses high surface wave velocity and satisfactorily large coupling coefficient, which enables high-frequency layered SAW devices applicable to telecommunications and sensing fields applications.

Acknowledgments: The author wishes to thank the Institute for Photonics and Nanotechnology, Rome Unit, who hosted her during the research period.

Conflicts of Interest: The author declares no conflict of interest.

References

1. Chung, G.-S.; Jeong, J.-M. Fabrication of micro heaters on polycrystalline 3C-SiC suspended membranes for gas sensors and their characteristics. *Microelectron. Eng.* **2010**, *87*, 2348–2352. [[CrossRef](#)]
2. Doppalapudi, D.; Mlcak, R.; Chan, J.; Tuller, H.; Bhattacharya, A.; Moustakas, T. MBE Grown AlN Films on SiC for Piezoelectric MEMS Sensors. In Proceedings of the MRS Symposium Y—GaN and Related Alloys, Boston, MA, USA, 1–5 December 2003; pp. 403–408.
3. Lin, C.; Chen, Y.; Felmetsger, V.V.; Lien, W.; Riekkinen, T.; Senesky, D.G.; Pisano, A.P. Surface acoustic wave devices on AlN/3C-SiC/Si multilayer structures. *J. Micromech. Microeng.* **2013**, *23*, 025019. [[CrossRef](#)]
4. Lin, C.; Chen, Y.; Pisano, A.P. Theoretical investigation of Lamb wave characteristics in AlN/3C-SiC composite membranes. *Appl. Phys. Lett.* **2010**, *97*, 193506. [[CrossRef](#)]
5. Caliendo, C. Theoretical investigation of Lamb wave A_0 mode in thin SiC/AlN membranes for sensing application in liquid media. *Sens. Actuators B Chem.* **2013**, *179*, 287–292. [[CrossRef](#)]
6. Liu, F.; Carraro, C.; Chu, J.; Maboudian, R. Residual stress characterization of polycrystalline 3C-SiC films on Si(100) deposited, from methylsilane. *J. Appl. Phys.* **2009**, *106*, 013505. [[CrossRef](#)]
7. Roper, C.S.; Howe, R.T.; Maboudian, R. Stress control of polycrystalline 3C-SiC films in a large-scale LPCVD reactor using 1,3-disilabutane and dichlorosilane as precursors. *J. Micromech. Microeng.* **2006**, *16*, 2736–2739. [[CrossRef](#)]
8. Lin, C.; Lien, W.; Felmetsger, V.V.; Hopcroft, M.A.; Senesky, D.G.; Pisano, A.P. AlN thin films grown on epitaxial 3C-SiC (100) for piezoelectric resonant devices. *Appl. Phys. Lett.* **2010**, *97*, 141907. [[CrossRef](#)]
9. Lin, C.; Chen, Y.; Felmetsger, V.; Senesky, D.; Pisano, A. AlN/3C-SiC composite plate enabling high frequency and high Q micromechanical resonators. *Adv. Mater.* **2012**, *24*, 2722–2727. [[CrossRef](#)] [[PubMed](#)]
10. Caliendo, C. Theoretical investigation of high velocity, temperature compensated Rayleigh waves along AlN/SiC substrates for high sensitivity mass sensors. *Appl. Phys. Lett.* **2012**, *100*, 021905. [[CrossRef](#)]
11. Adler, E.L. SAW and pseudo-SAW properties using matrix methods. *IEEE Trans. Ultrason. Ferroelect. Freq. Control* **1994**, *41*, 699–705. [[CrossRef](#)] [[PubMed](#)]
12. Farnell, G.W. Properties of elastic surface waves. In *Physical Acoustics, Principles and Methods*; Mason, W.P., Thurston, R.N., Eds.; Academic Press: New York, NY, USA, 1970; Volume VI, Chapter 4; p. 121.
13. Levinshtein, M.E.; Rumyantsev, S.L.; Shur, M.S. *Properties of Advanced Semiconductor Materials: GaN, AlN, InN, BN, SiC, SiGe*; Wiley: New York, NY, USA, 2001.
14. Collins, J.H.; Gerard, H.M.; Shaw, H.J. High performance lithium niobate acoustic surface wave transducers and delay lines. *Appl. Phys. Lett.* **1968**, *13*, 312–313. [[CrossRef](#)]
15. Ingebrigtsen, K.A. Surface waves in piezoelectrics. *J. Appl. Phys.* **1969**, *40*, 2681–2686. [[CrossRef](#)]
16. Tsubouchi, K.; Sugai, K.; Mikoshiba, N. AlN Material Constants Evaluation and SAW Properties on AlN/Al₂O₃ and AlN/Si. In Proceedings of the IEEE Ultrasonics Symposium, Chicago, IL, USA, 14–16 October 1981; pp. 375–380.
17. Hellwege, K.-H.; Hellwege, A.M. *Landolt-Börnstein, Numerical Data and Functional Relationships in Science and Technology, New Series, Group III*; Springer: Berlin, Germany, 1979.



© 2016 by the author; licensee MDPI, Basel, Switzerland. This article is an open access article distributed under the terms and conditions of the Creative Commons by Attribution (CC-BY) license (<http://creativecommons.org/licenses/by/4.0/>).